Showcasing research from Scott Mitchell's team at the Aragón Nanoscience and Materials Institute (INMA-CSIC/UNIZAR), Zaragoza, Spain.

Multifunctional polyoxomolybdate ionic liquid coatings for mitigating microbiologically influenced corrosion

Polyoxometalate-ionic liquids (POM-ILs) are applied as multifunctional coatings to combat microbiologically influenced corrosion of metal substrates. These materials provide long-lasting corrosion and biofouling resistance in highly acidic environments, maintaining stability over several months. This abstract artwork symbolizes the protection of metal surfaces. The dense, chaotic web of lines and splatters reflects the complex interplay between microbial activity and corrosion, while the vibrant ochre-yellow layer represents the protective POM-IL barrier, resisting the encroaching chaos of degradation. Image by Rafael González de Agüero.

Image reproduced by permission of Scott G. Mitchell and Rafael González de Agüero from *Mater. Horiz.*, 2025, **12**, 4648.

As featured in:

See Andrea Koerdt, Scott G. Mitchell *et al.*, *Mater. Horiz.*, 2025, **12**, 4648.

ROYAL SOCIETY OF CHEMISTRY

rsc.li/materials-horizons

Registered charity number: 207890

Materials Horizons

ROYAL SOCIETY OF CHEMISTRY

COMMUNICATION

View Article Online
View Journal | View Issue

Cite this: *Mater. Horiz.*, 2025, **12**, 4648

Received 2nd March 2025,
Accepted 7th May 2025

DOI: 10.1039/d5mh00373c

rsc.li/materials-horizons

Multifunctional polyoxomolybdate ionic liquid coatings for mitigating microbiologically influenced corrosion†

Mariella Malefioudaki, [a] Archismita Misra, [c] Nadja Sbeity, [c] Juan Zueco-Vincelle, [a] Miguel A. Laguna-Bercero, [a] Andrea Koerdt, *[c] Rafael Martín-Rapún [ab] and Scott G. Mitchell *[ab]

Corrosion of metals and other materials in marine environments poses significant economic, operational, safety, and environmental challenges across the oil and gas industry, the renewable energy sector, and maritime infrastructure. Microbiologically influenced corrosion (MIC) accounts for a substantial portion of this corrosion, with sulfate-reducing bacteria (SRB) and methanogenic archaea (MA) being key contributors. Conventional methods such as cathodic polarization have proven insufficient in mitigating the colonization of corrosive microbial communities in real marine environments, requiring the development of alternative, broad-spectrum antimicrobial strategies to prevent such biofilm formation. Recently, molybdate has emerged as a potential alternative to traditional biocides and nitrate. Our hypothesis is polyoxometalate-ionic liquids (POM-ILs), which exhibit antimicrobial and anticorrosion properties, could have a broader spectrum of antimicrobial activity than demonstrated until now and could be capable of shielding and protecting sensitive metal surfaces from the extreme acidic environments produced by MIC microorganisms. Here we show how two prototype polyoxomolybdate-based POM-ILs, $[(CH_3(CH_2)_6)_4N]_2[Mo_6O_{19}]$ and $[(CH_3(CH_2)_6)_4N]_4[Mo_8O_{26}]$, demonstrated antimicrobial activity at microgram per millilitre concentrations, prevented biofilm formation on metal surfaces, and provided resistance to corrosive acidic environments. Furthermore, impedance measurements were commensurate with electron microscopy studies showing that POM-IL-coated brass coupons withstood extremely corrosive environments. These proof-of-concept results demonstrate how multi-functional POM-IL coatings represent promising MIC mitigation solutions by providing a hydrophobic acid-resistant and biocidal protective layer that prevents biocolonisation and acidic corrosion by MIC microorganisms.

New concepts

This study reports the deployment of polyoxometalate-ionic liquids (POM-ILs) as novel multifunctional coatings to mitigate microbiologically influenced corrosion (MIC) of metal substrates. The results herein demonstrate how the cross-species antimicrobial activity of POM-ILs combined with their unique adaptable anticorrosive activity creates dual-action water-insoluble coatings that prevent microbial biofilm formation and protects metal surfaces from corrosion. Unlike traditional methods like cathodic polarization or chemical inhibitors which fail to address the complex interplay of microbial activity and corrosion in dynamic environments, POM-ILs offer robust corrosion protection in extreme highly acidic environments over several months. The exceptional protection they offer to metal surfaces is demonstrated by their ability to preserve brass alloy integrity under extreme corrosive conditions while preventing biofilm formation by sulfate-reducing bacteria and methanogenic archaea over a three-month period, as well as against real environmental samples. This research brings new insights into materials science by demonstrating the potential of POM-ILs to act as environmentally sustainable solutions that addresses the challenges interfacing corrosion and microbial activity. By expanding the utility of ionic liquid technologies and integrating them with molecular metal oxides, this work paves the way for next-generation coatings with applications across diverse industrial sectors.

Introduction

Corrosion is a chemical or electrochemical phenomenon causing deterioration and disintegration of materials. On metal/alloy surfaces it is the effect of unwanted chemical reactions resulting in the formation of more stable metal-oxides. In microbiologically influenced corrosion (MIC) the presence and metabolic activity of microorganisms accelerate

[a] *Instituto de Nanociencia y Materiales de Aragón (INMA-CSIC/UNIZAR), CSIC-Universidad de Zaragoza, C/Pedro Cerbuna 12, 50009 Zaragoza, Spain. E-mail: scott.mitchell@csic.es*

[b] *CIBER de Bioingeniería, Biomateriales y Nanomedicina, Instituto de Salud Carlos III, 28029 Madrid, Spain*

[c] *Bundesanstalt für Materialforschung und -prüfung (BAM), Department of Materials and Environment, Unter den Eichen 87, 12205 Berlin, Germany*

† Electronic supplementary information (ESI) available: Additional experimental details, data, figures and tables. See DOI: https://doi.org/10.1039/d5mh00373c

the corrosion of metals and alloys (other materials can be affected). Microorganisms such as bacteria, fungi, and archaea can colonize metal surfaces and create an environment that might promote corrosion. MIC can appear in various environments across different sectors and affect a broad variation of different materials, including water systems, soils, concrete, polymers, wood and industrial facilities to name just a few. The potential negative impact of microorganisms has been scientifically proven for several areas and materials and can be found, like microorganisms almost everywhere. Most of the knowledge on MIC has been gained from sectors related to energy production, storage, and infrastructure, such as oil and gas, marine industries, renewable energy, and water treatment. A NACE international impact study estimated the global cost of corrosion at US$2.5 trillion annually—marine corrosion alone costing an estimated US$50-80 billion annually—with MIC contributing to approximately 20% of all corrosion in aqueous systems.[1–3]

In general, two main types of MIC can be distinguished: (1) electronic MIC (E-MIC), in which microorganisms directly take up electrons from the metal surface and use them as electron donors (*e.g.* sulfate-reducing bacteria (SRB) facilitating cathodic depolarization); and (2) chemical MIC (C-MIC), where microorganisms produce or modulate chemical species that promote corrosion (*e.g.*, production of organic acids, hydrogen sulfide, concentration of chloride ions or other reactive components), but not necessarily by altering electron transfer directly.

The onset of MIC typically begins with the adhesion of microorganisms to a surface, followed by the development of a protective biofilm. This biofilm, composed of extracellular polymeric substances (EPS), acts as both a defensive barrier—shielding the microbial community from environmental stressors and toxic agents—and a selective filter that permits the diffusion of nutrients and metabolic byproducts. Within this microenvironment, microbial metabolic activity can dramatically alter local chemical conditions, accelerating metal dissolution and initiating corrosion processes.

Due to the highly localized nature of biofilm formation, MIC often leads to a non-uniform attack, resulting in damage that far exceeds that predicted by uniform corrosion models—sometimes reducing a structure's service life well below its original design parameters. When metals are the substrate, the situation becomes particularly critical. The electrochemical heterogeneity of the metal surface—where anodic and cathodic reactions occur at spatially separated sites—can promote pitting corrosion, a highly aggressive and localized form of attack. This can result in material failure far from the site of initial microbial activity. In critical infrastructure such as pipelines carrying flammable, toxic, or environmentally hazardous substances, such accelerated degradation can lead to catastrophic structural failures with severe safety and environmental consequences.[4–6]

Both aerobic and anaerobic microorganisms are involved in MIC, including sulfate-reducing bacteria (SRB), methanogenic archaea (MA), iron-oxidizer, iron-reducing microorganisms, and acetogenic microorganisms, among others.[7] In anaerobic environments, SRB utilize sulfate as a terminal electron acceptor in place of oxygen, oxidizing organic substrates into organic acids and carbon dioxide while reducing sulfate to hydrogen sulfide (H_2S). The generation of H_2S poses serious challenges, as it readily reacts with various materials, often leading to corrosion. To date, research has primarily focused on metals—particularly iron—due to their critical role in infrastructure and industry. During MIC processes involving metals, metallic ions such as Fe^{2+} are released into the environment. These ions can react with biogenic sulfide to form poorly soluble ferrous sulfide (FeS) precipitates, which often accumulate as corrosive deposits on material surfaces.[8] In the case of metals, MIC presents an additional challenge: ferrous sulfide (FeS), a common corrosion product formed by the reaction between Fe^{2+} and biogenic sulfide, is electrically conductive. This conductivity facilitates continued electron transfer at the metal surface, thereby sustaining and potentially accelerating the corrosion process. Another important group of MIC-associated microorganisms are methanogenic archaea (MA), which thrive on substrates associated with the terminal stages of the carbon cycle, including H_2/CO_2, acetate, methanol, and methylamines. Their metabolic end product is methane—a potent greenhouse gas with a significantly higher global warming potential than carbon dioxide. Notably, some methanogenic strains have evolved mechanisms to bypass conventional hydrogen metabolism. These electroactive methanogens are capable of directly accepting electrons from metallic surfaces and scavenging protons from the surrounding environment to generate hydrogen *in situ*. The locally produced hydrogen then fuels methanogenesis, further promoting MIC through a self-sustaining, bioelectrochemical feedback loop.[9]

Copper and its alloys are extensively used in various applications, including domestic and industrial pipeline systems, heat exchangers, fire sprinkler systems, and marine structures. This is due to their excellent machinability, thermal and electrical conductivity, ease of soldering, and corrosion resistance (as they are used even as a biocidal agent[10–12]). The formation of a protective patina on copper surfaces in the presence of oxygen enhances corrosion resistance by creating a passivating layer. Despite their long history as antibacterial and antimicrobial agents, copper – and particularly its alloys – are highly susceptible to microbial colonization and biodeterioration.[10–12] Numerous cases of MIC have been reported for copper and its alloys, often resulting in significant infrastructure failures.[12,13] Brass is a copper alloy composed primarily of copper and zinc, but one which often includes varying amounts of other metals like lead, tin, or iron to enhance its properties. Alpha (α) brass, characterized by a single-phase microstructure containing less than 37% zinc, is widely valued for its excellent cold-workability and inherent corrosion resistance. Despite these advantageous properties, α brass—like other copper-based alloys—is still susceptible to MIC, particularly in environments where microbial activity can alter local electrochemical conditions. Such corrosion can undermine the structural integrity of the material over time, limiting its long-term performance in critical applications.[14,15]

Several techniques are currently being used for the control, prevention, and inhibition of MIC. One of the most common techniques is cathodic polarization (CP). CP reduces the corrosion of a metal structure by making it the cathode of an electrochemical cell, using either a more active sacrificial anode or by impressing a current with an external direct current source. However, the effect of CP is still under discussion, since the current is not evenly distributed over the whole surface and the impact metabolic products (like acids) can have, is still unclear (especially in underground or sediment areas of a material).[16–19]

The effectiveness of the traditional techniques remains uncertain, particularly in complex dynamic environments, such as marine and wastewater systems where sampling and testing are difficult or even impossible. Recently, molybdate anions have demonstrated their effectiveness in inhibiting the growth of SRB and have been shown to reduce microbial souring in batch reactions.[20] Furthermore, polyaniline–molybdate has been used to prevent corrosion on steel surfaces.[21]

Polyoxometalates (POMs) are a diverse class of nanoscale molecular metal oxides, with a wide and versatile range of physicochemical properties that can be tuned on the molecular level. POMs are composed of early transition metals from groups V and VI in their highest oxidation states, commonly V^V, Mo^{VI} and W^{VI}. The rich redox chemistry and diverse oxidation states of POMs means that they also display antimicrobial activity.[22–24] Moreover, ionic liquids (ILs), which are salts with melting points below 100 °C have demonstrated excellent performance as anticorrosive agents through coating formation and lubrication.[25–27] The greatest advantage of ILs is their modular design, which allows the cation and anion to be adjusted separately, thereby tailoring the formation of multifunctional materials that are appropriate for surface coatings.

Polyoxometalate-ionic liquids (POM-ILs), room-temperature ionic liquids formed from POM anions with bulky organic cations such as alkylammonium or -phosphonium,[28] have gained significant attention in the area of surface-active IL coatings due to their exceptional chemical reactivity and versatility.[29] Such POM-Ils have been used to great effect as coatings for natural stone, preventing corrosion and biodeterioration.[30]

Our hypothesis was that complex polyoxomolybdate-based POM-ILs could prove to be an innovative chemical solution for this emerging environmental and industrial problem. In this way, we demonstrate that the spectrum of activity and application of POM-ILs can be transferred to between sectors (*e.g.*, heritage conservation and water purification) and materials (*e.g.*, stone and metal surfaces). Furthermore, by doing so we demonstrate that POM-ILs have a broader "spectrum of action" than originally imagined. Here we report the synthesis and characterization of polyoxomolybdates transformed into POM-Ils using a tetraheptylammonium cation, which are used subsequently as hydrophobic, anticorrosive, and antimicrobial coatings (a cross-species effect) to prevent MIC of metal surfaces (Fig. 1).

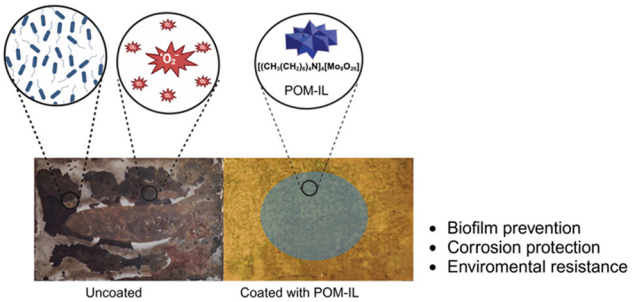

Fig. 1 Overview of the general approach and objective.

Results and discussion

Synthesis and characterization of polyoxomolybdate-ionic liquids (POM-ILs)

Two polyoxomolybdate ionic liquids (POM-ILs) were synthesized utilizing the distinct properties of molybdate anions and tetraheptylammonium cations. The POM-ILs were synthesized through an aqueous "one pot" self-assembly method by acidifying a solution of molybdate(VI) building blocks, followed by the addition of a molar excess of tetraheptylammonium ($THEPA^+$) bromide. This general approach was used for the formation of POM-Ils, $[(CH_3(CH_2)_6)_4N]_2[Mo_6O_{19}]$ (**Mo_6**) and $[(CH_3(CH_2)_6)_4N]_4[Mo_8O_{26}]$ (**Mo8**).

Briefly, for the synthesis of **Mo_6**, $THEPA^+$ was added to an aqueous sodium molybdate solution adjusted to pH 5.5, under continuous stirring. This resulted in the formation of $[(CH_3(CH_2)_6)_4N]_2[Mo_6O_{19}]$, appearing as a dark green gel-like substance. The **Mo_6** Lindqvist structure is composed of four octahedrally coordinated $[MoO_6]$ units in a belt region, capped by Mo atoms on the top and bottom, yielding an overall octahedral symmetry. The synthesis of **Mo_8** followed an identical protocol, with the variation being the adjustment to pH 4, which yielded $[(CH_3(CH_2)_6)_4N]_4[Mo_8O_{26}]$ as a bright yellow gel-like substance. The $[Mo_8O_{26}]$ structure features a six-membered ring of octahedral $[MoO_6]$ units, capped on both sides by two $\{MoO_4\}$ tetrahedra.[31]

The synthesized POM-Ils were characterized using Fourier transform infrared spectroscopy (FT-IR), Thermogravimetric analysis (TGA), and elemental analysis to confirm their composition and purity (Table S1, ESI†). The FT-IR spectra of the two POM-ILs exhibited characteristic absorption bands for the POM. Specifically, the bands at 954 and 795 cm^{-1} correspond to Mo═O and Mo–O–Mo, respectively. The presence of tetraheptylammonium was verified by the presence of the C–H stretching bands at 2957 and 2871 cm^{-1}, which are assigned to ν(C–H) stretching vibrations in the aliphatic alkyl chains. The bending vibrations of CH_2 and CH_3 groups are observed in the range of 1400–1480 cm^{-1}, corresponding to $\delta(CH_2)$, $\delta_{as}(CH_3)$, and $\delta_s(CH_3)$ modes (Fig. 2).[32,33] Thermogravimetric analysis (TGA) provided insights into the thermal stability and the distribution between the organic and inorganic components of the POM-ILs. Both materials were stable up to at least 190 °C. Subsequent weight losses were ascribed to the decomposition of $THEPA^+$ cations, the organic part of the material.

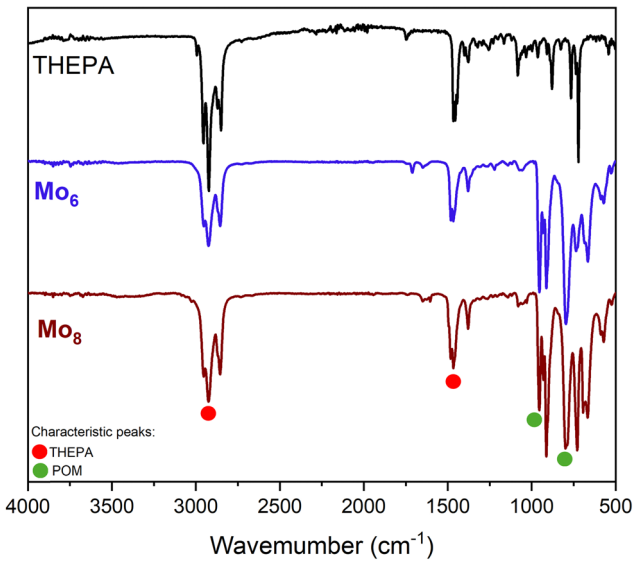

Fig. 2 FT-IR spectra of THEPABr, **Mo$_6$** and **Mo$_8$**.

For **Mo$_6$** and **Mo$_8$**, the weight losses of the organic portion of the POM-ILs at 400 °C of 50.68% and 59.35% aligned with the corresponding theoretical value of 48% and 58%, respectively (Fig. S1 and S2, ESI†).

Antimicrobial activity of POM-ILs

The antimicrobial properties of POM-ILs were evaluated against Gram-positive (*Bacillus subtilis* and *Staphylococcus epidermidis*) and Gram-negative (*Escherichia coli*) model organisms. These model organisms were chosen to facilitate rapid assessment of the antimicrobial activity of POM-ILs in a laboratory setting, providing preliminary data before extensive screening against specific MIC microorganisms, like sulfate-reducing bacteria (SRB) and methanogenic archaea (MA).

The experimental protocol involved using a 96-well plate assay. Bacteria were cultured in appropriate media (*E. coli* in Luria-Bertani and *B. subtilis* and *S. epidermidis* in Nutrient Broth) and exposed to serial dilutions of POM-ILs in 2% dimethylsulfoxide (DMSO) (Fig. S6, ESI†). Bacterial viability was evaluated using a resazurin-based colorimetric assay, where resazurin (blue) is reduced to resorufin (pink) by metabolically active cells.[34] The concentration of POM-ILs inhibiting bacterial growth was determined by the absence of color change (Fig. S7, ESI†).

Table 1 Minimum bactericidal concentration (MBC) of POM-ILs against *E. coli*, *B. subtilis* and *S. epidermidis*[a]

Minimum bactericidal concentration (MBC) (μg mL^{-1})			
Bacteria	*E. coli*	*B. subtilis*	*S. epidermidis*
Mo$_6$	3.5	0.6	0.4
Mo$_8$	4.0	0.4	0.4

[a] Resazurin cell viability assays were confirmed by colony counting of aliquots seeded on agar plates (refer to Experimental section).

Table 1 presents the corresponding minimum bactericidal concentrations (MBCs) of the POM-ILs against three model bacterial strains, *E. coli*, *B. subtilis*, and *S. epidermidis*. The higher MBC values for *E. coli* are due to structural differences between Gram-negative and Gram-positive bacteria. Gram-negative bacteria have approx. 2.5–4 nm peptidoglycan cell wall and an outer membrane, while Gram-positive bacteria have thicker (approx. 30–100 nm) layers of peptidoglycan.[35] POM-ILs exert antimicrobial effects primarily through electrostatic interactions with negatively charged bacterial cell surfaces. These interactions likely disrupt membrane integrity, leading to cell death. Gram-positive bacteria, with their porous peptidoglycan walls, are generally more susceptible, whereas Gram-negative bacteria require higher concentrations due to their protective outer membrane.[36]

Metal surface antimicrobial activity

The surface antimicrobial activity of **Mo$_6$** and **Mo$_8$** on α-brass coupons (35ZN,65CU) were tested to evaluate the capacity of the POM-IL coatings to prevent biofilm formation on these surfaces. A modified JIS Z 2801 standard method (Fig. S8, ESI†), commonly used for evaluating antimicrobial properties on non-porous substrates, was used to evaluate the ability of the POM-ILs to prevent bacterial adhesion and the subsequent formation of biofilms. *E. coli* as a Gram-negative model known for its capacity to form biofilms, as well as its resilience and resistance to antimicrobial agents, and *S. epidermidis* as a Gram-positive model, making them an appropriate choice for assessing the effectiveness of the POM-ILs in the metal surfaces.

To determine the extent of bacterial reduction, the number of bacterial colonies on the metal samples coated with POM-ILs was compared to the number of colonies on uncoated samples. The metal surfaces were coated with 80 μL of 40 mg mL^{-1} concentration for **Mo$_6$** and **Mo$_8$**. The results showed that at these concentrations there was a 100% reduction of bacterial growth on all metal surfaces for both bacteria strains (Table S3, ESI†).

Further analysis using scanning electron microscopy (SEM) was conducted to observe the effect of POM-ILs on the metal surfaces. The SEM images of the uncoated brass samples (Fig. 3a) showed significant biofilm formation on the surface after 48 hours. In contrast, the brass samples coated with POM-

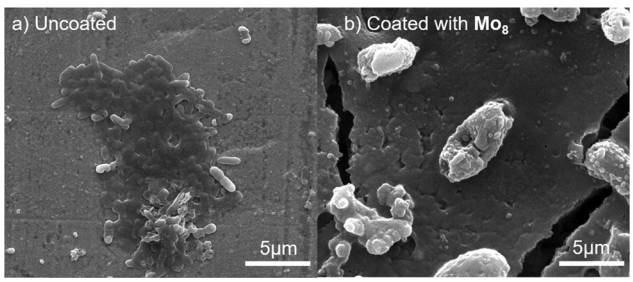

Fig. 3 SEM images of an *E. coli* biofilm growth in LB medium for 48 hours on: (a) the uncoated brass coupon; (b) brass coupon coated with 40 mg mL^{-1} of **Mo$_8$**.

ILs (Fig. 3b) displayed non-viable bacterial cells and cell components dispersed on the surface, indicating an effective prevention of biofilm formation.

Anticorrosive activity of POM-ILs

Inspired by previous studies in which insoluble solid POM-salts were employed as corrosion inhibitors,[28] the anticorrosion activity of $\mathbf{Mo_6}$ and $\mathbf{Mo_8}$ was evaluated using brass coupons (15 mm × 20 mm × 1 mm), which were coated with 80 μL of 40 mg mL^{-1} of POM-ILs. These brass coupons were then exposed to aqueous acetic acid 10% for different periods and compared with control samples containing no POM-IL coating (Fig. S9, ESI†). Acetic acid was chosen as a model to simulate volatile corrosive agents commonly found in the environmental corrosion of metals such as iron, brass, and copper.[37] All samples were washed with acetone and distilled water to remove residual POM-IL coating, ensuring that only the effects of the initial coating were assessed. SEM was performed to investigate the effects of POM-IL coatings on brass coupons and on the exposed samples (Fig. 4). SEM and photo analysis revealed significant differences between the coated and uncoated brass coupons across all exposure times. The uncoated samples displayed extensive surface damage and corrosion, with visible signs of copper and zinc oxidation. The degree of corrosion increased with longer exposure times. In contrast, the POM-IL coated samples showed markedly less corrosion, with far fewer distortions and signs of deterioration. The EDX analysis supported these observations by confirming the elemental composition of the surface of the brass coupons (Fig. S10 and S11, ESI†). The uncoated samples showed significant signs of copper and zinc corrosion, whereas the coated samples exhibited fewer signs of corrosion products.

Impedance analysis of POM-IL-coated brass coupons

Electrochemical impedance spectroscopy (EIS) was used to analyze the anticorrosion mechanisms of $\mathbf{Mo_6}$ and $\mathbf{Mo_8}$-coated brass coupons (Fig. S12, ESI†). Two types of samples were tested: coated and uncoated brass coupons, both before and after exposure to 10% acetic acid for 24 hours. After exposure, the corroded layer and any remaining coatings were removed. The Nyquist impedance plots (Fig. 5e and f) provided insights into the effectiveness of the coatings. Higher values of real (Z') and imaginary (Z'') impedance components indicated better anticorrosion activity. Both Z' and Z'' increased with frequency, though the rise in Z'' was more limited. The increase in Z' suggested enhanced charge transfer resistance, correlating with improved anticorrosion performance.[38–40]

EIS data were fitted using two different electrical equivalent circuit (EEC) models: one for uncoated samples and coated samples measured after exposure and cleaning (Fig. 5a), and another for non-exposed coated samples, which retained the coating for the EIS measurements (Fig. 5b). For exposed and cleaned samples, a model with three parallel RCPE (resistance-constant phase element) components was used. The first RCPE at high frequency attributed to the natural brass patina, the second to charge transfer resistance, and the third to the diffusion of corrosion products (Fig. 5a and Table 2). For coated samples (Fig. 5b and Table 3), additional elements were

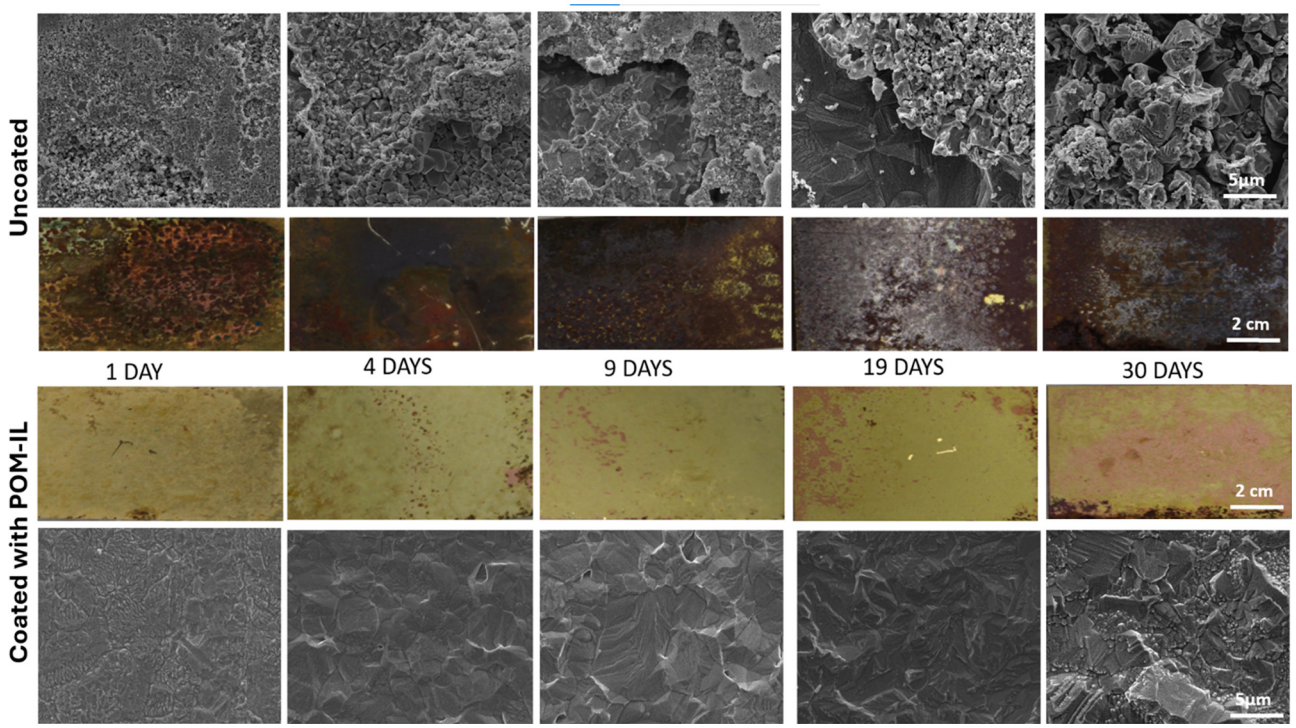

Fig. 4 SEM (10 000× magnification) and photographic images of uncoated and POM-IL-coated brass coupons after exposure to 10% of aqueous acetic acid vapour for 1, 4, 9, 19, and 30 days.

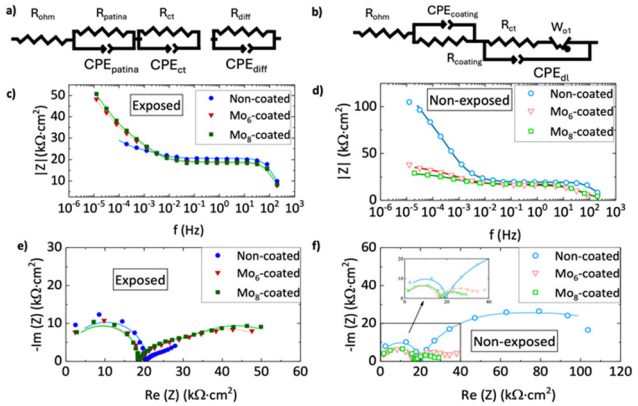

Fig. 5 (a) Equivalent electrical circuit (EEC) model for brass coupons which had been exposed to aqueous acetic acid 10% for 24 h and cleaned (POM-IL coating removed if present) before EIS measurement; (b) EEC model for samples which were not exposed to aqueous acetic acid 10% for 24 h (non-exposed); (c) and (e) Bode and Nyquist plots for brass coupons which were exposed to aqueous acetic acid 10% for 24 h and cleaned (POM-IL coating removed if present); (d) and (f) Bode and Nyquist plots for non-exposed samples.

included to represent coating resistance ($R_{coating}$) and capacitance ($CPE_{coating}$), as well as charge transfer resistance (R_{ct}) and double-layer capacitance (CPE_{dl}), with the Warburg element describing diffusion through the coating.[41,42]

In the first model (Fig. 5a and Table 2), as corrosion of brass is mainly associated with zinc depletion, no significant change was observed in the first contribution (patina), which is related to the copper carbonate surface layer. However, a clear decrease in the R_{ct} value was observed when going from non-exposed to exposed samples, indicating increased corrosion activity after exposure. This decrease was less pronounced in coated samples, demonstrating the protective effect of the coatings. Moreover, coated samples also exhibited higher diffusion resistance (third element) than the uncoated ones, though still lower than under non-exposed conditions.[42]

The second model was used to fit the results for coated samples which were neither exposed to acidic environment nor cleaned, that is, the coating was present during the EIS measurements (Fig. 5b and Table 3). Similar Warburg resistance (Wo_R) and *T*-parameters were obtained across coated samples, suggesting that the diffusion of corrosion products through the coating pores is comparable. These results are summarized in Tables 2 and 3.

Bode plots (Fig. 5c and d) complemented this analysis, showing low conductivity at lower frequencies for coated samples after the exposure, a sign of effective corrosion protection.[41,42] Overall, the EIS analysis confirmed that both **Mo_6** and **Mo_8** coatings offered substantial protection, with **Mo_8**-coated samples showing particularly strong resistance to the corrosive environment.

Preventing microbially influenced corrosion

So far it has been demonstrated that POM-ILs possess remarkable anticorrosion and antimicrobial properties against aerobic microorganisms and being water-insoluble, they do not leach into aquatic ecosystems, which is extremely valuable for environmental sustainability and to beneficial organisms. However, their performance against anaerobic microorganisms has never been explored. This would be important as anaerobic environments are at the highest risk for MIC. This study aimed to develop an optimized methodology to coat the metal surface with POM-ILs and achieve protection against MIC-relevant microorganisms. The effectiveness of the POM-IL coating on brass alloys was tested against the MIC-causing methanogenic microorganisms, specifically *Methanococcus maripaludis* Mic1c10, as well as SRB such as *Desulfovibrio ferrophilus* IS5 and *Oleidesulfovibrio alaskensis* DSM 16109, formerly known as *Desulfovibrio alaskensis* (Table 4). MIC on metal is typically categorized by two general mechanisms: electrical MIC (E-MIC) and chemical MIC (C-MIC). In E-MIC, microorganisms engage with the metal surfaces, utilizing them as direct or indirect electron source for their metabolism, thereby ensuring their survival by boosting their energy metabolism. Some studies further distinguish E-MIC based on the mechanism of electron uptake.[18] Direct E-MIC involves physical contact with the metal surface (*e.g.* surface protein or pili), while indirect E-MIC requires electron-transfer-mediators released from microorganisms (special enzymes or other kind of shuttle). These mediators utilize electrons from the metal either directly or produce substances such as H_2, which are released into the environment and used as electron donor indirectly; however, the latter can potentially be utilized by other species. In C-MIC, corrosion is driven by microorganisms producing corrosive metabolites, including protons, organic acids, chloride ions, and sulfur species.[9] Unlike E-MIC, C-MIC does not necessitate a biocatalyst. Corrosive metabolites undergo reduction on the metal surface, with proton reduction potentially occurring concurrently with metal oxidation under sufficiently low pH conditions. SRB have garnered significant attention due to their well-understood mechanism involving the reduction of sulfate ions (SO_4^{2-}) to hydrogen sulfide (H_2S), a corrosive acid.[43] An example of such bacteria is *Desulfovibrio ferrophilus* IS5, known for its ability to accelerate the corrosion of carbon steel.[44] This

Table 2 Results of resistances and peak frequencies between brackets of each contribution to Nyquist diagram obtained for cleaned samples (non-coated samples or samples in which the coating was removed for the EIS measurements)

Metal sample	R_{patina} (Ω cm²) (f–kHz)	R_{ct} (Ω cm²) (f–Hz)	R_{diff} (Ω cm²) (f–mHz)
Uncoated + non-exposed	1.99×10^4 (13.9)	5.50×10^4 (0.4)	6.31×10^4 (19.5)
Uncoated + exposed	2.11×10^4 (14.9)	3.63×10^3 (3.2)	1.62×10^4 (32.7)
Mo_6-coated + exposed	1.95×10^4 (13.7)	8.90×10^3 (1.6)	3.04×10^4 (23.0)
Mo_8-coated + exposed	1.91×10^4 (14.1)	1.06×10^4 (1.4)	3.27×10^4 (20.9)

Table 3 Results of resistances and peak frequencies and Warburg resistance with its T-parameter between brackets of each contribution to the Nyquist diagram

Samples	$R_{coating}$ (Ω cm^2) (f–kHz)	R_{ct} (Ω cm^2) (f–Hz)	Wo_R (Ω cm^2) (T–s)
Mo_6-coated + non-exposed	1.68×10^4 (34.2)	1.88×10^4 (0.70)	9.98×10^3 (78.15)
Mo_8-coated + non-exposed	1.80×10^4 (32.7)	1.04×10^4 (0.74)	5.62×10^3 (68.80)

Table 4 Experimental overview for MIC-prevention experiments on brass coupons

Experimental Conditions	Experiment 1 (E1)	Experiment 2 (E2)
Media	Artificial sea water supplemented with 1 M sulfate	Artificial sea water supplemented with 1 M lactate and 1 M sulfate
Microorganism	*Desulfovibrio ferrophilus* IS5	*Methanococcus maripaludis* (Mic1c10) and *Oleidesulfovibrio alaskensis* 16109
Incubation period	Thirteen weeks	Eight weeks

lithographically grown microorganism is particularly notorious for causing severe MIC in seawater environments.[45] An interesting feature of *Methanococcus maripaludis* strain is that it has the ability for both E-MIC and C-MIC.[46,47] Methanogens usually need at least H_2 or CO_2 for their normal metabolism and produce methane. Some methanogens can cause corrosion *via* the so-called MIC-hydrogenase. In this case they secrete hydrogenase, which most likely attach to the metal surface an withdraw electron from the surface and convert it together with proton or the surrounding environment to H_2. This H_2 is then used, like in the standard methanogenesis, as an electron donor and together with CO_2, methane is formed. As SRBs mainly cause MIC *via* C-MIC and some strains of methanogens can proceed *via* both E-MIC and C-MIC pathways, a mixture of both type of microorganisms was used in Experiment 2 to observe their combined biocorrosive effect on coated and uncoated metal coupons. Among the tested POM-ILs, **Mo_8** was selected for its higher organic content, which likely contributes to a denser, more hydrophobic coating. The elevated concentration of tetraheptylammonium cations not only enhances antimicrobial activity but also improves barrier protection. These qualities, along with its superior performance in initial trials, made **Mo_8** the rational choice for further experiments and to streamline subsequent testing.

Two experiments were carried out to evaluate the effectiveness of POM-IL as a protective coating against MIC on brass coupons. In Experiment 1, sulfate-supplemented artificial seawater was inoculated with *D. ferrophilus* IS5 and six samples were prepared: three with POM-IL coating and three without used as controls. In Experiment 2, artificial seawater was supplemented with lactate (10 mL, 1 M) and sulfate (15 mL, 1 M) and inoculated with a mixture of 2.5 mL of the SRB *Oleidesulfovibrio alaskensis* 16109 preculture and 2.5 mL of the MA *Methanococcus maripaludis* Mic1c10 preculture in a similar setup as described before. All experiments were conducted under anaerobic, sterile conditions in which all equipment was sterilized and headspaces were flushed with N_2/CO_2 to maintain an oxygen-free environment and avoid contamination.

Visual inspection revealed a distinct contrast between the POM-IL coated and uncoated coupons in both experiments. The surface of the POM-IL-coated coupons (Fig. 6c and g) almost retained their original appearance in terms of color, surface integrity and brightness, whereas the uncoated ones (Fig. 6b and f) exhibited evident surface attack and deterioration. Upon closer examination of the sample surfaces, for the coupons coated with POM-IL maintained a consistent surface, similar in smoothness to the initial state. In contrast, the uncoated coupons exhibited substantial disparities in color, surface structure, and observable rough features on the surface.

In Experiment 1, SEM images of uncoated coupons exposed to *Desulfovibrio ferrophilus* IS5 (Fig. 6a) revealed a complex biofilm development, characterized by a heterogeneous surface with elevated regions and flaky corrosion byproducts, potentially metal oxides originating from artificial seawater (ASW) medium. In contrast, coated samples (Fig. 6d) exhibited a relatively homogeneous surface with occasional cracks and sparse corrosion byproducts near these cracks, suggesting the formation of a protective passivation layer by the POM-IL coating, which limited microbial attachment and surface degradation. Quantitatively, uncoated samples showed a weight loss of 0.087% and a corrosion rate of 0.003 mm year^{-1}, compared to the coated samples with a significantly reduced weight loss of 0.009% and a corrosion rate of 0.0003 mm year^{-1}, indicating nearly 10 times of reduction in corrosion (Table 5).

In Experiment 2, SEM imaging of uncoated coupons exposed to a mixture of *Methanococcus maripaludis* and *Desulfovibrio alaskensis* (Fig. 5e) showed flaky corrosion products, cylindrical bacterial cells, and a visibly uneven surface, all indicative of biofilm formation and extensive surface damage. Coated samples (Fig. 5h) displayed a protective layer, however, with small surface cracks, where corrosion byproducts such as copper and zinc oxides (confirmed by EDX spot analyses) were localized at the edges of these cracks rather than uniformly distributed. Additionally, dispersed non-viable bacterial cells and cellular components were observed, suggesting a reduced ability for biofilm formation on the coated surfaces.

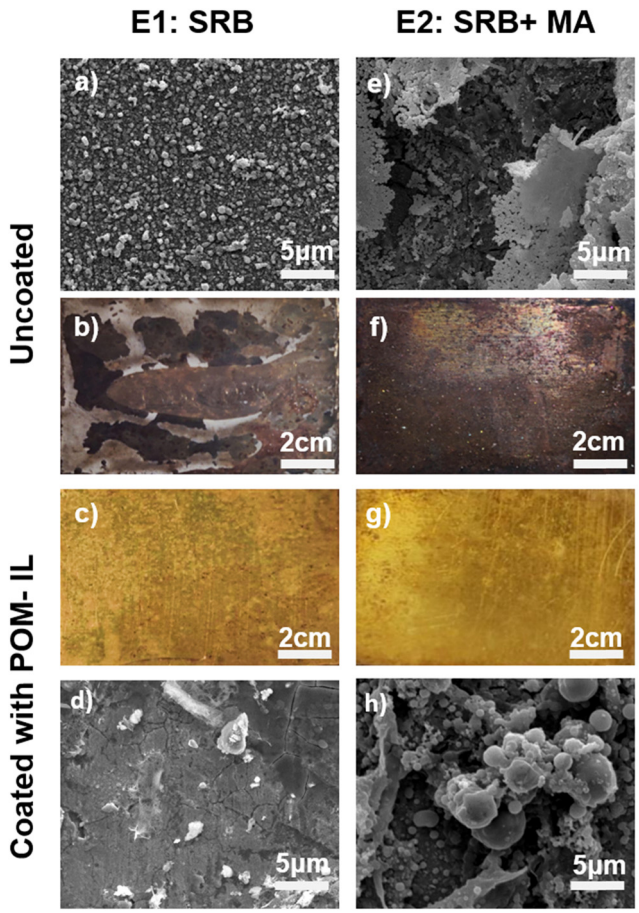

Fig. 6 SEM images (12 000× magnification) and photographs of uncoated and **Mo_8**-coated brass coupons after incubation in artificial seawater (ASW) media: (a)–(d) with sulfate-reducing bacteria (SRB) *Desulfovibrio ferrophilus* IS5 for 13 weeks, and (e)–(h) with a 1 : 1 mixture of methanogenic archaea (MA) *Methanococcus maripaludis* Mic1c10 and SRB *Oleidesulfovibrio alaskensis* 16109 for eight weeks.

Table 5 Weight loss estimation of uncoated and **Mo_8**-coated brass coupons after incubation in artificial seawater (ASW) media: (E1) *with Desulfovibrio ferrophilus* IS5 for 13 weeks, and (E2) with a 1 : 1 mixture of *Methanococcus maripaludis* Mic1c10 and *Oleidesulfovibrio alaskensis* 16109 for eight weeks

Sample	Initial weight (g)	Final weight (g)	Weight loss (%)	Corrosion rate (mm year^{-1})
E1 Uncoated	2.0536	2.0518	0.087	0.003
E1 Coated	2.0630	2.0628	0.009	0.0003
E2 Uncoated	2.0985	2.0920	0.309	0.0167
E2 Coated	2.0969	2.0959	0.047	0.0026

Weight-loss measurements showed that uncoated samples suffered 0.309% weight loss and a corrosion rate of 0.017 mm year^{-1}, while coated samples had significantly lower values of 0.047% and 0.003 mm year^{-1}, respectively, demonstrating a six-times reduction in corrosion (Table 5).

The corrosion rates of four commonly used biocidal treatments in the oil and gas industry, specifically against *Desulfovibrio ferrophilus* IS5, are illustrated in (Fig. S13, ESI†), derived from previously published literature.[48] Among these, POM-IL exhibited the lowest corrosion rate, at 0.003 mm year^{-1}. Tetrakis(hydroxymethyl)phosphonium sulfate (THPS) followed with a corrosion rate of 0.025 mm year^{-1}. A combination of glutaraldehyde (GLUT) and benzalkonium chloride (BAC) demonstrated a higher corrosion rate of 0.15 mm year^{-1}, while glutaraldehyde (GLUT) alone resulted in the highest corrosion rate of 0.44 mm year^{-1}. These data highlight the efficacy of POM-IL in comparison to more traditional biocidal treatments.

Environmental sediments

To assess the influence of environmental microorganisms on microbiologically influenced corrosion (MIC), sediment samples were collected from Schlachtensee, Berlin, Germany. The sampling process utilized sterilized syringes to extract sediment from various depths and locations around the lake's shoreline (Fig. S14, ESI†), ranging from areas near visible biomass to those with distinct odors indicative of sulfate-reducing bacteria (SRB) activity. After collection, syringes were sealed with sterile parafilm and stored in anaerobic jars filled with CO_2, which displaced oxygen to maintain anaerobic conditions critical for preserving microbial composition. This process minimized environmental alterations, ensuring accurate representation of the *in situ* microbial communities.

Such sediments are expected to host diverse microorganisms, including SRB and methanogens. The sediment samples were introduced into controlled environments alongside brass coupons, coated and uncoated with POM-IL. Results revealed a stark contrast between biotic (microorganism-containing) and abiotic (sterilized) sediment samples. Uncoated coupons displayed significant surface degradation, with biotic samples exhibiting higher corrosion rates than their abiotic counterparts. Notably, sediment with active microbial communities produced higher concentrations of dissolved sulfide, corroborating the metabolic activity of SRB within these environments.

In the biotic samples, high sulfide concentrations were observed due to SRB activity, with uncoated samples exhibiting sulfide levels of up to 0.106 mM (Table S4, ESI†). This directly correlated with elevated corrosion rates in the uncoated coupons (Table S5, ESI†). For example, the uncoated biotic brass samples showed corrosion rates exceeding 3.47×10^{-3} mm year^{-1}, demonstrating significant material degradation within just 13 weeks of exposure. In contrast, POM-IL-coated coupons significantly mitigated these effects. Coated biotic samples displayed reduced sulfide concentrations (as low as 0.087 mM) and halved corrosion rates (1.58×10^{-3} mm year^{-1}), highlighting the ability of the coating to inhibit microbial activity and protect the underlying metal surface. Further experiments along this line are already planned to optimize and establish the efficacy of POM-IL coatings in the context of environmental samples.

SEM analysis revealed distinct differences between biotic and abiotic samples, both coated and uncoated. In the biotic, uncoated sample (Fig. 7a), dense biofilm structures and extensive surface pitting were observed, accompanied by visible corrosion byproducts such as sulfides, indicating aggressive

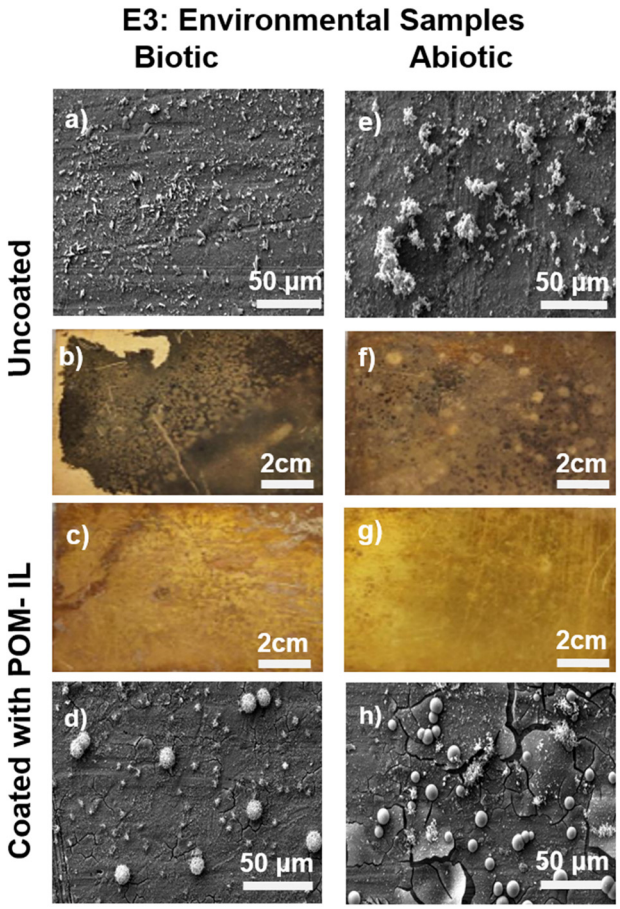

Fig. 7 SEM images (3000× magnification) and photographs of uncoated and Mo_8-coated brass coupons after incubation in freshwater media: (a)–(d) with microbial communities inhabiting sediment from Schlachtensee, Berlin, for 13 weeks, and (e)–(h) in abiotic freshwater media for 13 weeks.

microbial activity. The presence of repetitive cylindrical structures, resembling microorganisms, and high sulfur concentrations further suggested the involvement of SRB in the corrosion process. In contrast, the biotic, coated sample (Fig. 7d) showed a more homogeneous surface with minimal biofilm formation and reduced pitting.

In the abiotic, uncoated sample (Fig. 7e), cloudy corrosion products were evident, likely the result of chemical corrosion or mineral precipitation, with no signs of biological activity. On the other hand, the abiotic, coated sample (Fig. 7h) displayed copper/zinc oxides in the form of white round shapes, confirming the protective role of the coatings against oxidation. While some cracking of the POM-IL layer was noted, it did not significantly compromise the protection, and the surface showed far less corrosion compared to the uncoated sample, demonstrating the efficacy of the coating in mitigating chemical degradation.

These results demonstrate the dual functionality of POM-IL coatings in mitigating MIC: (1) reducing microbial colonization and sulfide production, and (2) providing a physical barrier that inhibits chemical and microbial-induced surface degradation. This is especially significant in environments rich in sediments where microbial activity is highly concentrated, such as marine or freshwater systems.

Although laboratory MIC systems cannot fully replicate the unpredictable and multifactorial nature of real environmental settings, they provide a robust platform for assessing protective materials under representative conditions. The current endeavors simulate different biocorrosive environments using environmental samples and mixed microbial consortia to evaluate the efficacy of POM-IL nanocoatings on metal surfaces. The findings serve as a scientifically relevant foundation for future studies aiming to incorporate broader and more dynamic and even codependent environmental variables.

Conclusions

Here we have demonstrated the effectiveness of polyoxometalate ionic liquid (POM-IL) coatings to mitigate microbiologically influenced corrosion (MIC). The antimicrobial activity of the POM-ILs was assessed using model MIC-inducing microorganisms including sulfate-reducing bacteria and methanogenic archaea. Through diverse analytical methods, including corrosion rate assessments, SEM and electrochemical analysis, we gained valuable insights into the efficacy of POM-IL coatings in industrial settings where MIC is a concern.

Our findings indicate that POM-IL coatings effectively protect brass coupons exposed to acidic environments for one month and embedded in environmental sediment over a three-month period. Coated samples exhibited significantly less surface damage and maintained their integrity compared to uncoated samples, demonstrating the ability of POM-IL coatings to inhibit corrosion and microbial colonization. SEM analysis showed that POM-IL coatings reduced surface irregularities and the formation of corrosion products, further underscoring their protective capabilities. Additionally, POM-IL coatings were effective at inhibiting sulfate-reducing bacteria activity, as evidenced by lower sulfide concentrations in coated samples, indicating cross-species biocidal activity. Despite these promising results, we also identified some limitations, SEM images revealed occasional cracking post-exposure. These cracks likely stem from mechanical stress during the drying process, as well as fluctuations in temperature and humidity during storage or testing. Since POM-ILs are applied as relatively soft films that evaporate solvents, they can develop internal tension when the solvent (acetone) evaporates quickly, leading to shrinkage and minor fissures. In environments where temperature or humidity varies, the differences in thermal expansion between the brass substrate and the POM-IL layer might also play a role in crack formation.

Although these cracks did not significantly affect the short-term performance of the coating (as confirmed through corrosion data and SEM analysis), they could potentially allow corrosive agents or microorganisms to penetrate over time, which might reduce the long-term protective effectiveness of the POM-IL layer. As such, our on-going research efforts are currently focused on optimizing the protective properties of

POM-IL coatings and validating their applicability in real-world scenarios, for instance, by incorporating POM-ILs into polymeric supports to improve their long-term performance and durability. This mixed strategy aims to merge the antimicrobial and anticorrosive benefits of POM-ILs with the mechanical strength of traditional polymers. We believe that overcoming such practical obstacles could enable POM-IL coatings to become a robust and reliable solution for corrosion mitigation in various industrial and cultural contexts.

Experimental section

Synthesis of tetraheptylammonium hexamolybdate(VI), $([CH_3(CH_2)_6]_4N)_2[Mo_6O_{19}]$ (Mo_6)

$6Na_2MoO_4 + 10HCl + 2[CH_3(CH_2)_6]_4NBr \rightarrow ([CH_3(CH_2)_6]_4N)_2(Mo_6O_{19}) + 10NaCl + 2NaBr + 5H_2O$

In an Erlenmeyer flask, 10 g (0.04 mol) of sodium molybdate dihydrate ($Na_2MoO_4{\cdot}2H_2O$) was dissolved in 40 mL of water. The solution was acidified by adding 11.6 mL of 6 N hydrochloric acid (HCl) and stirred vigorously for 1 min at room temperature. To the acidified sodium molybdate solution, a separate solution of 7.30 g (0.01 mol) of tetraheptylammonium bromide $[CH_3(CH_2)_6]_4NBr$ in 8 mL of water was added with vigorous stirring. The addition resulted in the formation of a white precipitate. The resulting slurry was heated to a temperature range of 75 to 85 °C and stirred for 45 min. During this process, the white solid changed to a green color. The light green particles were separated from the solution through filtration, and subsequent washing was performed with water to remove any residual impurities. The washed particles were then dried under vacuum conditions to ensure complete solvent removal. The dried light green particles were dissolved in 30 mL of toluene. The toluene was evaporated on a rotary evaporator and the resulting dark green complex was collected as the total product. Yield: 10.6 g, 90% (based on Mo). FT-IR (cm^{-1}): 2957 and 2871 cm^{-1} (ν(C–H)), 1400–1480 cm^{-1} ($\delta(CH_2)$, $\delta_{as}(CH_3)$, $\delta_s(CH_3)$), 954 cm^{-1} (Mo═O), and 795 cm^{-1} (Mo–O–Mo). TGA expt. (calc.): 50.68% (48%). CHN expt. (calc.)%: C: 41.9 (39.5), H 6.9 (7.1), N 1.7 (1.6).

Synthesis of tetraheptylammonium octamolybdate (VI), $([CH_3(CH_2)_6]_4N)_4[Mo_8O_{26}]$ (Mo_8)

$8Na_2MoO_4 + 12HCl + 4[CH_3(CH_2)_6]_4NBr \rightarrow ([CH_3(CH_2)_6]_4N)_4[Mo_8O_{26}] + 12NaCl + 4NaBr + 6H_2O$

In a 100 mL beaker, 10 g (0.04 mol) of commercial sodium molybdate dihydrate was dissolved in 24 mL of water. The solution was then acidified by adding 10.4 mL of 6 N aqueous HCl, and vigorous stirring was maintained over a period of 2 min at room temperature. A solution of 10.16 g (0.02 mol) of tetraheptylammonium bromide in 30 mL of toluene was prepared in a separate container. The tetraheptylammonium bromide solution was added to the acidified sodium molybdate solution with vigorous stirring, and the mixture was stirred for 25 min resulting in a yellow solution, which was then transferred to a vacuum rotary evaporator in order to remove the remaining toluene solvent, leaving the final yellow product. Yield: 10.8 g, 76% (based on Mo). FT-IR (cm^{-1}): 2957 and 2871 cm^{-1} (ν(C–H)), 1400–1480 cm^{-1} ($\delta(CH_2)$, $\delta as(CH_3)$, $\delta s(CH_3)$), 954 cm^{-1} (Mo═O), and 795 cm^{-1} (Mo–O–Mo). TGA expt. (calc.): 59.35% (58%). CHN expt. (calc.)%: C 51.6 (47.6), H 8.5 (8.6), N 2.1 (2.0).

Bacterial growth inhibition and cell viability assays

The study of each POM-IL involved using 96-well plates and following a specific protocol. On Day 1, a 1 : 20 dilution of 1×10^7 CFU mL^{-1} bacteria was prepared by adding 500 μL of a saturated bacteria solution to 9.5 mL of medium in a T-25 flask, using Luria–Bertani broth (LB) for *E. coli* and Nutrient Broth (NB) for *B. subtilis* and *S. epidermidis*. The POM-IL compounds were diluted, ranging from 50 to 0.2 μg mL^{-1} with each concentration diluted in half for a first estimation of the MIC and for more precise 5 μg mL^{-1} to 1 μg mL^{-1} for *E. coli* (step size of 0.5 μg mL^{-1}) and from 0.9 to 0.1 μg mL^{-1} for *B. subtilis* and *S. epidermidis* (step size of 0.1 μg mL^{-1}). Each well of the 96-well plate received 98 μL of the respective medium, with a control (−) receiving 200 μL of medium and a control (+) receiving 100 μL of medium and 100 μL of the 1 : 20 dilution of bacteria. Additionally, 2 μL of the diluted POM-IL compounds were added to each well, along with 100 μL of the 1 : 20 dilution of bacteria. The plate was then incubated for 24 h at 37 °C. On Day 2, after the incubation period, 20 μL of 0.1 mg mL^{-1} of Resazurin (7-hydroxy-3*H*-phenoxazin-3-one 10-oxide) sodium salt in the corresponding medium was added to each well. Resazurin (blue) is irreversibly reduced to the pink-colored and highly red fluorescent resorufin by dehydrogenase enzymes in metabolically active cells.[34] Therefore, pink wells after the corresponding incubation time indicate live, viable bacteria, whereas blue wells indicate a loss of metabolic activity, which is one of the first cascade events in the mechanism of cell death. The bacterial viability was verified by subculturing 100 μL of each well on solid media for colony plate counting. After incubating the plates for 24 h at 37 °C, the minimum bactericidal concentration (MBC) values obtained with Resazurin were compared with the lack of colonies in the solid media.

Surface antimicrobial activity

The modified JIS Z 2801 standard (Reference number: JIS Z 2801:2000 (E); ICS 07.100.10; 11.100) was used to study the surface antimicrobial activity. The experimental procedure spanned three days. 15 × 20 mm sized α-brass (35ZN,65CU) metal coupons (sterilized 70% ethanol and UV light) were coated with POM-ILs dissolved in acetone at 40 mg mL^{-1}. On the first day, a bacterial suspension with approximately 10^7 CFU mL^{-1} was prepared. Then, 50 μL of this suspension was applied to the surface of the metal sample of interest which had been coated with the desired concentrations of POM-IL and to a reference sample without any antimicrobial activity. A coverslip was placed over 50 μL of bacterial suspension on all the samples to ensure uniform contact. Subsequently, the samples were placed in a humid chamber (a glass container

of wet paper with distilled water) and incubated at 37 °C for 24 h. On the second day, after the 24-hour incubation period, the bacteria present in the samples were extracted into a liquid medium. This was achieved by transferring the samples into a 50 mL Falcon tube containing 15 mL of culture media and vortexing them for 1 minute. The culture media with the extracted bacteria, was then diluted and plated onto agar plates. The agar plates were subsequently incubated at 37 °C for 24 h. On the last day (day 3), the colony-forming units (CFU) on the cultivated agar plates were counted. The percentage of bacterial growth reduction was obtained by comparing the number of colonies present in the plates from the coated samples and the colonies present in the plates from the control sample. To calculate the value of the antimicrobial activity, the following formula (1) was employed: log reduction = log(CFU reference sample) − log(CFU antimicrobial sample).

Corrosion of metal coupons

Brass metal coupons (15 × 20 mm) were coated 80 μL with 40 mg mL^{-1} concentrations of $\mathbf{Mo_6}$ and Mo_8 (diluted in acetone). Subsequently, the POM-IL-coated metal surfaces, along with an uncoated reference sample (without POM-IL), were exposed to 10% aqueous acetic acid vapour during 1, 3, 9, 19 and 30 days. The exposure took place in a glass case filled with 40 mL of the corresponding diluted aqueous acetic acid, where the metal samples were placed on the inverted glass vials (not immersed in the acidic solutions). Following a 24-h exposure, the metal coupons were collected and washed using distilled water and acetone to remove residues.

Bacteria cell fixation for SEM analysis

The brass coupons were first sterilized under UV light for 20 min and then coated with 80 μL of POM-IL at a concentration of 40 μL mL^{-1}. The coated coupons were placed in a 6-well plate, with 3 mL of a 1 : 20 dilution of bacterial culture of 1×10^7 CFU per mL, and incubated for 48 h at 37 °C. After incubation, the coupons were washed twice with 2 mL of sterile physiological saline solution (SFE). Subsequently, 2 mL of 2.5% glutaraldehyde in 0.1 M cacodylate buffer was added to each well, and the samples were incubated for 1 h at 37 °C This was followed by three washes with 2 mL of distilled water. The samples were dehydrated with a 30% methanol for 5 min, followed by a 50% methanol for 5 min, before being dried in air. The dried and fixed samples were stored in a refrigerator until the following day, whereupon the samples were coated with palladium (Pd) for visualization using SEM.

Preparation of artificial sea water (ASW) media for incubation tests with MIC-relevant microorganisms

Preparing a medium derived from seawater proves effective nurturing for *Desulfovibrio ferrophilus* IS5, *Oleidesulfovibrio alaskensis*, and *Methanococcus maripaludis*. This involves creating an artificial seawater (ASW) medium supplemented with tailored additives to foster the growth of these bacteria.[49]

Seawater media were prepared for experiments 1 and 2 (Table 4). To prepare 1L ASW a sterile container was filled with 1L Milli-Q water. The media was supplemented with the following salts: 0.45 mol (26.37 g) of NaCl, 0.12 mol (11.20 g) of $MgCl_2$, 0.01 mol (1.48 g) of $CaCl_2$ and 0.008 mol (0.60 g) KCl under stirring conditions to dissolve completely. After complete dissolution of all the salts, the pH was adjusted with Na_2CO_3 to 7.2. Subsequently, the medium was sterilized by autoclaving at 121 °C for 15 min. After cooling down the media to room temperature other minerals and other heat sensitive components *e.g.* vitamins, were added to create a well-balanced and nutrient-rich environment that supports the growth and metabolic activities of specific microorganisms in the media.

Ammonium chloride (NH_4Cl, 3.74 M, 1.25 mL) and potassium dihydrogen phosphate (KH_2PO_4, 1.10 M, 1.33 mL) were added to enhance the salinity and phosphate content. To support microbial metabolism, sodium bicarbonate ($NaHCO_3$) at 1 M concentration (60 mL) was included as a carbon source. Additionally, trace elements without EDTA from FMU (1 mL), Se-Wo (1 mL), and 5-vitamins from FMU (1 mL) were added to provide essential micronutrients. For cofactor and vitamin supplementation, lipoic acid + folic acid (1 mL), thiamine at a concentration of 0.1 mg mL^{-1} (1 mL), riboflavin at a concentration of 0.025 g mL^{-1} (1 mL), and vitamin B12 at a concentration of 0.05 mg mL^{-1} (1 mL) were added. To create reducing conditions in the media, sodium sulfide (Na_2S) at 1 M concentration (1 mL) and cysteine (1 mL) were included. Lastly, acetate (1 mL) was incorporated to serve as an additional carbon and energy source for microbial growth. These supplements collectively contribute to the optimal nutritional environment for the targeted microorganisms within the media. For experiment 1 : 15 mL of Na_2SO_4 (1 M) was added. For the experiment 2 : 10 mL lactate (1 M) and 15 mL Na_2SO_4 (1 M) were added. Lactate was supplemented to act as an electron donor. Sulfate was added to act as an electron acceptor in anaerobic respiration of SRB, where they reduce sulfate to sulfide.

Experimental setup

Two experiments were designed to investigate the hypothesis regarding the efficacy of POM-IL as a protective coating on brass coupons against MIC. In Experiment 1, sulfate-supplemented artificial seawater was prepared and inoculated with *D. ferrophilus* IS5. Six samples were then prepared: three containing the brass coupons coated with POM-IL and three coupons without the coating as the control. All samples were subsequently inoculated with the microorganism. In experiment 2, artificial seawater media was again utilized and supplemented with lactate and sulfate. Two different microorganisms were introduced in ratio 1 : 1: a sulfate-reducing bacterium, *Oleidesulfovibrio alaskensis* 16109, and a methanogenic archaea, *Methanococcus maripaludis* Mic1c10. Six samples were prepared, of which three were coated and three were not. For the preparation of the flasks every necessary equipment was sterilized. This process was performed under anaerobic and sterile working conditions to ensured that any potential contaminants were eliminated like airborne bacteria and archaea. For flushing of the headspace syringes containing N_2/CO_2 were used to ensure the oxygen-free environment.

Preparation of pre- culture for experiment 2

For experiment 2, four sterilized flasks were filled with ASW media supplemented with lactate and Na_2SO_4. One flask was inoculated with 5 mL *M. maripaludis* Mic1c10, including a carbon steel coupon, and another flask with the same microorganism but a brass coupon instead. A third flask, containing ASW media, was inoculated with 5 mL *Oleidesulfovibrio alaskensis* 16109 and a carbon steel coupon, while the fourth flask, also with 5 mL *Oleidesulfovibrio alaskensis* 16109, had a brass coupon. Subsequently, all flasks were placed in an incubator at 37 °C for a duration of 2 weeks to facilitate growth.

Coating of brass coupons with POM-ILs

To achieve 40 mg mL^{-1} concentration of POM-IL, 400 mg of the Mo_8 POM-IL was diluted with 10 mL of acetone. The brass coupons (15 mm × 20 mm × 1 mm) were sterilized first with ethanol and then under UV light for 30 min (15 min for each side) inside a clean bench and weighed to document the initial weight. Next, they were coated with 80 μL of the prepared POM-IL in acetone solution using a pipette by spreading it evenly on the metal surface to ensure uniform coverage on the coupons. The coupons underwent a coating process where they were drop-coated and then allowed to dry for a short period of time.

Inoculating the flasks with microorganisms

For experiment 1 *Desulfovibrio ferrophilus* IS5 was added to all six flasks containing the coated and uncoated coupons. For experiment 2, 2.5 mL of a preculture with *M. maripaludis* (Mic1c10) and 2.5 mL of *Desulfovibrio alaskensis* Da16109 (prepared with brass coupons), were added to the flasks containing either coated or uncoated brass coupons.

Final assembly for experiment 1. Six Schott flasks (100 mL each) were filled with 50 mL artificial sea-water media, the coated and uncoated brass coupons and the headspace of the flasks were flushed with N_2/CO_2 for at least 3 min. Lastly, they were put into an incubator at 30 °C.

Final assembly for experiment 2. Six Schott flasks (100 mL) were prepared with 50 mL artificial seawater media and the coated and uncoated brass coupons, and the headspace was flushed with N_2/CO_2 for 3 min. First, they were stored at RT. After two weeks the precultures were injected inside the samples. The samples as well as the precultures were sent to incubate at 30 °C.

Post-incubation treatment of the coupons

Coupon washing for visual inspection and weight loss estimation. Initially, the coupons needed to undergo a washing process with a *N*, *N*′ – Dibutylthiourea (DBT) + HCl/dH_2O solution in a 1 : 1 ratio. The coupons were transferred from flasks to six-well plates. The washing procedure involved pipetting out 1 mL of the solution onto each coupon, followed by placing them on a shaker for precisely ten min. Subsequently, the acidic washing solution was quickly removed using a pipette. To neutralize, 1 mL of $NaHCO_3$ (1 M) solution was added on top and left for 5 min. Using tweezers, the coupons were then rinsed first with Milli-Q water and then acetone and finally dried with N_2. These were then photographed, and the weight loss was calculated.

Preparations for scanning electron microscopy (SEM). To prepare coupons for SEM, they were washed with a 1 : 2 buffer solution of 1× PBS (phosphate-buffered saline)/dH_2O. Initially, the coupons were moved from flasks to six-well plates, and 1 mL of the solution was applied to each using a pipette. Subsequently, the excess solution was removed. For cellular fixation, 1 mL of 2.5% glutaraldehyde solution was added to the coupons, which were then refrigerated at 4 °C overnight. The following day, the samples underwent a wash with 1× PBS/dH_2O for 5 min, followed by an additional 5-minute wash in dH_2O. Dehydration was achieved by successive additions of 30% (30 min), 50% (30 min), 70% (30 min), 80% (60 min), 90% (60 min), and absolute ethanol (60 min) over the next 4.5 hours. Lastly, the samples were dried with N_2 and stored in a six well plate, wrapped with parafilm and stored inside a desiccator at RT. After this procedure the coupons underwent gold coating (thickness = 15 nm) using a Quorum Q150R ES Rotary pumped coater in order to make the surface conductive for SEM.

Weight loss estimation. In order to quantify the corrosion rate (CR), formula (1) was used.

$$\mathrm{CR} = \frac{K \times m_{\mathrm{loss}}}{A \times t \times \rho} \quad (1)$$

where, K is a constant 8.76 × 104 so that CR is in [mm $year^{-1}$], m_{loss} is the mass loss [g] of the metal ($m_0 - m_f$) in time t [hours], A is the surface area of the material exposed [cm^2], and ρ is the density of the material [g cm^{-3}], ρ_{Brass} = 8.47 g cm^{-3}.[50]

Author contributions

Conceptualisation – SGM, AK & RMR; methodology – all authors; investigation – MM (POM-IL synthesis & characterization, antibacterial assays, anticorrosion experiments, and SEM characterization) JZV (electrochemistry) & AM (environmental studies and microbiologically influenced corrosion experiments); data curation – all authors; writing, original draft – MM, JZV & AM; writing, review & editing – all authors; supervision – SGM, RMR, AK & MLB. project administration; SGM & RMR; funding acquisition – SGM & RMR.

Data availability

The datasets supporting this article have been uploaded as part of the supplementary information. The corresponding author Scott G. Mitchell can also be contacted for specific enquiries.

Conflicts of interest

There are no conflicts to declare.

Acknowledgements

This work was funded through the grants PID2022-141276OB-I00, PID2022-137626OB-C31 and CEX2023-001286-S funded by MCIN/AEI/10.13039/501100011033 (Ministerio de Ciencia e Innovación/Agencia Estatal de Investigación, Spain). This study was supported by MCIN with funding from the European Union NextGenerationEU (PRTR-C17.I1) promoted by the Government of Aragón. The authors also acknowledge Fondo Social del Gobierno de Aragón (grupo DGA E15_23R and T02_23R). The authors acknowledge the Servicio General de Apoyo a la Investigación-SAI (Universidad de Zaragoza), for the use of instrumentation as well as the technical advice provided by the National Facility ELECMI ICTS, node ''Laboratorio de Microscopías Avanzadas'' at the University of Zaragoza. This work was supported by COST (European Cooperation in Science and Technology) and based upon work from COST Action European MIC Network—New paths for science, sustainability and standards (Euro-MIC) [CA20130].

References

1 H. Ma, W. Zhang, Y. Wang, Y. Ai and W. Zheng, *Saf. Environ. Prot.*, 2023, **171**, 71–86.
2 Y. K. Cai, Y. Zhao, Z. K. Zhang, X. B. Ma and B. Cheng, Atmospheric and marine corrosion: influential environmental factors and models, *In Proceedings of the International Workshop on Environmental Management, Science and Engineering*, 2018, pp. 178–186.
3 G. Koch, *Trends Oil Gas Corros. Res. Technol.*, 2017, **3**, 3–30.
4 M. Seter, M. J. Thomson, J. Stoimenovski, D. R. MacFarlane and M. Forsyth, *Chem. Commun.*, 2012, **48**, 5983–5985.
5 S. T. Kalajahi, A. Misra and A. Koerdt, *Frontal Nanotechnol.*, 2024, **6**, 1340352.
6 P. Rao and L. Mulky, *J. Bio Tribo Corros.*, 2023, **9**, 57.
7 B. A. An, E. Deland and A. Koerdt, *NACE Corrosion*, 2021, D111S046R001.
8 Z. Li, J. Yang, S. Lu, W. Dou and T. Gu, *J. Mater. Res. Technol.*, 2023, **27**, 3777–3787.
9 B. A. An, S. Kleinbub, O. Ozcan and A. Koerdt, *Front. Microbiol.*, 2020, **11**, 527.
10 N. D. Güngör, A. Çotuk and D. Dışpınar, *J. Mater. Eng. Perform.*, 2015, **24**, 1357–1364.
11 S. Chen, P. Wang and D. Zhang, *Corros. Sci.*, 2014, **87**, 407–415.
12 R. Amendola and A. Acharjee, *Front. Microbiol.*, 2022, **13**, 806688.
13 M. A. Javed, W. Neil, G. Adam and S. A. Wade, *Corros. Prev.*, 2016, **84**, 1–14.
14 M. L. Carvalho, J. Doma, M. Sztyler, I. Beech and P. Cristiani, *Bioelectrochemistry*, 2014, **97**, 2–6.
15 M. Rkayae, M. Ebn Touhami, Y. Baymou, Y. Hassani, K. Elgoufifa and M. Allam, *J. Bio Tribo Corros.*, 2022, **8**, 62.
16 B. J. Little, D. J. Blackwood, J. Hinks, F. M. Lauro, E. Marsili, A. Okamoto and H. C. Flemming, *Corros. Sci.*, 2020, **170**, 108641.
17 M. S. Khan, T. Liang, Y. Liu, Y. Shi, H. Zhang, H. Li and Y. Zhao, *Metals*, 2022, **12**, 1458.
18 J. Knisz, R. Eckert, L. M. Gieg, A. Koerdt, J. S. Lee, E. R. Silva and S. A. Wade, *FEMS Microbiol. Rev.*, 2023, **47**, fuad041.
19 Y. K. Cai, Y. Zhao, Z. K. Zhang, X. B. Ma and B. Cheng, Atmospheric and marine corrosion: influential environmental factors and models, *In Proceedings of the International Workshop on Environmental Management, Science and Engineering*, 2018, pp. 178–186.
20 F. Kögler, F. S. Hartmann, D. Schulze-Makuch, A. Herold, H. Alkan and N. Dopffel, *Int. Biodeterior. Biodegrad.*, 2021, **157**, 105158.
21 V. Karpakam, K. Kamaraj, S. Sathiyanarayanan, G. Venkatachari and S. Ramu, *Electrochim. Acta*, 2011, **56**, 2165–2173.
22 L. L. Liu, L. Wang, X. Y. Xiao, P. Yang, J. Zhao and U. Kortz, *Coord. Chem. Rev.*, 2024, **506**, 215687.
23 L. Guo, L. He, Q. Zhuang, B. Li, C. Wang, Y. Lv and Y. F. Song, *Small*, 2023, **19**, 2207315.
24 L. Cronin and A. Müller, *Chem. Soc. Rev.*, 2012, **41**, 7333–7334.
25 C. Verma, E. E. Ebenso and M. A. Quraishi, *J. Mol. Liq.*, 2017, **233**, 403–414.
26 M. Seter, M. J. Thomson, J. Stoimenovski, D. R. MacFarlane and M. Forsyth, *Chem. Commun.*, 2012, **48**, 5983–5985.
27 E. K. Ardakani, E. Kowsari, A. Ehsani and S. Ramakrishna, *Microchem. J.*, 2021, **165**, 106049.
28 S. Herrmann, M. Kostrzewa, A. Wierschem and C. Streb, *Angew. Chem., Int. Ed.*, 2014, **53**, 13596–13599.
29 K. Rajkowska, A. Koziróg, A. Otlewska, M. Piotrowska, E. Atrián-Blasco, I. Franco-Castillo and S. G. Mitchell, *Molecules*, 2020, **25**, 5663.
30 A. Misra, I. Franco Castillo, D. P. Müller, C. Gonzalez, S. Eyssautier-Chuine, A. Ziegler, J. M. de la Fuente, S. G. Mitchell and C. Streb, *Angew. Chem., Int. Ed.*, 2018, **57**, 14926–14931.
31 W. G. Klemperer, *Inorg. Synth.*, 1990, **27**, 74–85.
32 Y. K. Al-Majedy, H. H. Ibraheem, L. S. Jassim and A. A. Al-Amiery, *Al-Nahrain J. Sci.*, 2019, **22**, 1–8.
33 M. E. S. Mirghani, I. Y. Qudsieh and F. A. Elfaki, *IIUM Eng. J.*, 2008, **9**, 27–38.
34 K. Präbst, H. Engelhardt, S. Ringgeler and H. Hübner, *Methods Mol. Biol.*, 2017, **1601**, 1.
35 A. G. Enderle, I. Franco-Castillo, E. Atrián-Blasco, R. Martín-Rapún, L. Lizarraga, M. J. Culzoni and S. G. Mitchell, *ACS Appl. Polym. Mater.*, 2022, **4**, 4144–4153.
36 A. Bijelic, M. Aureliano and A. Rompel, *Chem. Commun.*, 2018, **54**, 1153–1169.
37 A. López-Delgado, E. Cano, J. M. Bastidas and F. A. López, *J. Electrochem. Soc.*, 1998, **145**, 4140.
38 P. L. Bonora, F. Deflorian and L. Fedrizzi, *Electrochim. Acta*, 1996, **41**, 1073–1082.
39 H. H. Hernández, A. R. Reynoso, J. T. González, C. G. Morán, J. M. Hernández, A. M. Ruiz and R. O. Cruz, *Electrochem. Impedance Spectrosc.*, 2020, 137–144.
40 B. Ramírez Barat and E. Cano, *ChemElectroChem*, 2018, **5**, 2698–2716.

41 S. Qiu, C. Chen, M. Cui, W. Li, H. Zhao and L. Wang, *Appl. Surf. Sci.*, 2017, **407**, 213–222.
42 J. Gong, H. Wei, P. Hao, S. Li, X. Zhao, Y. Tang and Y. Zuo, *Materials*, 2024, **17**, 378.
43 J. Telegdi, A. Shaban and L. Trif, *Trends Oil Gas Corros. Res. Technol.*, 2017, 191.
44 D. Wang, P. Kijkla, M. E. Mohamed, M. A. Saleh, S. Kumseranee, S. Punpruk and T. Gu, *Bioelectrochemistry*, 2021, **142**, 107920.
45 M. Chatterjee, Y. Fan, F. Cao, A. A. Jones, G. Pilloni and X. Zhang, *Sci. Rep.*, 2021, **11**, 15458.
46 S. T. Lohner, J. S. Deutzmann, B. E. Logan, J. Leigh and A. M. Spormann, *ISME J.*, 2014, **8**, 1673.
47 F. Mayer, B. Sabel-Becker and D. Holtmann, *Microorganisms*, 2022, **10**(11), 2237.
48 M. Sharma, H. Liu, S. Chen, F. Cheng, G. Voordouw and L. Gieg, *Sci. Rep.*, 2018, **8**, 16620.
49 E. A. Ghazy, M. G. Mahmoud, M. S. Asker, M. N. Mahmoud, M. M. Abo Elsoud and M. E. Abdel Sami, *J. Am. Sci.*, 2011, **7**, 604–608.
50 F. Malaret and X. S. Yang, *Exp. Results*, 2022, **3**, e13.